Aeroelastic Tailoring using Rib/Spar Orientations: Experimental Investigation

G. Francois[1], J. E. Cooper[2] and P. M. Weaver[3]
Department of Aerospace Engineering, University of Bristol, Bristol, BS8 1TR, U.K.

Wing aeroelastic performance, such as static aeroelastic shape, flutter/divergence speed and gust load response, has a critical impact on aircraft design and consequently the tailoring of aeroelastic response offers much potential for weight savings. In this paper, the configuration between the spars and ribs of an un-tapered, un-swept wing box is varied to modify the aeroelastic performance. Different spar/rib orientations are investigated through numerical simulation and an experimental test program using 3D printed wings. A series of static and dynamic wind-off and wind tunnel tests show that it is possible to have a significant influence on the structural behaviour.

I. Introduction

Today's commercial aviation is predicted to see a growth of 5% per annum until at least 2030[1]. Such a promising future is nonetheless facing some issues amongst which the industry's fossil fuel dependency is one of the biggest. The improvement in engine fuel efficiency has started to flatten, forcing aircraft designers to find efficiency improvements by focusing on the overall aircraft and reducing structural weight and drag. These goals require that future aircraft be optimised and designed with rules where tradition does not override success.

The science of aeroelasticity focuses on the excitation and deformation of a structure under the interaction of elastic, aerodynamic and inertial forces[2]. The aeroelastic performance of aircraft wings has been considered for many years in the design process as a certification requirement so as to avoid flutter/divergence and a catastrophic failure during a gust encounter[2], often resulting in penalising the design through the addition of weight. Aeroelasticity also dictates the deformation shape of the wing in-flight affecting the drag produced by the aircraft; the wing "jig-shape" is designed to that the optimal aerodynamic shape is obtained at the cruise flight condition. Challenged with the need to improve aircraft efficiency, aeroelastic performance is becoming a key design driver so as to reduce the amount of structure used by the wing, for flutter/divergence and gust response control, and by tailoring wing deformation during the entire flight envelope to reduce drag. Understanding the different methods by which aeroelastic performance can be controlled is therefore important to aircraft designers.

Aeroelastic tailoring has been primarily researched using composite materials to influence the coupling of bending and torsion motions through control of material anisotropic properties[3]. The use of coupling phenomenon through either stacking sequence optimisation[4–8] or novel manufacturing methods[9,10] have shown the possibility of a large positive impact on the aeroelastic performance. However, the idea of aeroelastic tailoring has mainly been investigated on conventional structural designs[6,7].

In addition to aeroelastic tailoring through composite tailoring, aeroelastic performance can be improved through the use of novel wing internal structural designs. This has been highlighted by research in wing structural optimisation which encompasses: (1) topology optimization and (2) shape optimisation.

Topology optimization focuses on finding the optimal number and shape of structural features[11]. Significant improvement in aeroelastic tailoring have been achieved through the development of novel wing structure by research work using the Solid Isotropic Material with Penalization[12] (SIMP) method or the Level Set[13,14] method. Kolonay and Kobayashi[15] who used a cellular division method to perform topology, shape and sizing optimisation of a fighter aircraft wing box showed similar improvements in aeroelastic tailoring. However, aeroelastic tailoring achieved through the topology optimisation often generates complex solutions often hardly transferable into real designs.

[1] PhD Research Student
[2] Royal Academy of Engineering Airbus Sir George White Professor of Aerospace Engineering, AFAIAA
[3] Professor in Lightweight Structures

An alternative approach to structural aeroelastic tailoring is structure shape optimisation where the initial number and positions of the structural members are specified and set, but can change shape as part of the design process. The possibility offered by shape optimisation was first presented by Harmin *et al*[16] who modified the angles between the ribs and the spars to generate bend-twist coupling on an aluminium wing to improve the aeroelastic performance. When considering composite wings, Vio and Fitzpatrick[17] optimised the shape of a straight un-tapered composite wing box. The optimisation looked at modifying the spars shape using a Genetic Algorithm (GA) by moving the nodes position in a cell-discretised wing box structure. The analysis showed the possibility of controlling instability speed, mass and gust response in an advantageous manner by controlling the structural shape. Later Vio *et al*[8] explored further this concepts of wing box deformation by fitting third order Non-Uniform Rational B-Splines (NURBS) to the rear and front spar of a sweptback tapered wing box. The optimised design was seen to be different to straight spars/ribs structure design and had improved mass, instability speed and gust response. Finally, Francois and Cooper[18] showed that the significant improvement in flutter speed and gust response could be achieved by modifying the shape of a straight wing box through the use of curved spars and/or ribs.

Similarly, Locatelli *et al*[19] showed that the use of curved spars and ribs allowed a reduction of the weight of a wing-box when subjected to stress and buckling constraints. Their approach decoupled the spars and ribs curvatures from the rib/spar arrangement allowing for more realistic wing design. Later Liu *et al*[19] performed a two-step optimisation of the aluminium NASA Common Research Model (CRM) wing to minimise its structural weight while subject to flutter speed, stress and buckling constraints in a static aeroelastic calculations. Significant weight savings were achieved while aeroelastic constraints were met. Jutte *et al*[10] used curvilinear spars and ribs to perform aeroelastic tailoring on a composite NASA CRM wing when considering flutter speed and stresses during a static aeroelastic analysis. Although this work did not consider the optimising of the solution, it highlighted that significant aeroelastic performance gains can be achieved through the use of curvilinear spars and ribs. Finally Francois *et al*[20] showed that curved spars and ribs in a reduced design freedom framework resulted in wings with improved flutter speed while meeting buckling and stress constraints on both backward and forward swept wings.

Past research in aeroelastic tailoring have shown that improvements in aeroelastic performances are achieved by a positive change in the structural coupling phenomenon such as the creation of twist through the application of bending loads. Although research work has highlighted the benefits that novel wing structural design can offer in aeroelastic tailoring, understanding the mechanism by which novel structural design changes the structural coupling behaviour remains to be established. Additionally this has never been illustrated experimentally.

In this paper, the impact of the rib/spar arrangement on aeroelastic performance is investigated both numerically and experimentally through consideration of different rib/spar arrangements. The numerical and experimental tests include static testing, wind tunnel testing and dynamic testing using wings manufactured using polyamide laser sintering.

This paper is structured as follows: Section II described the concept explored and the wing geometry considered then Section III describes the structural modelling performed. Section IV details the experimental part of this paper. Finally Section V shows the modelling and experimental results and Section VI concludes this paper.

II. Concepts and Wing Model Considered

A. Concept

This paper explores the impact of the orientation of the ribs with respect to the spars (rib/spar arrangement) on the aeroelastic performance of a wing. Interestingly very little information exist regarding the impact of the rib/spar arrangement. Classic structural design textbooks[21] limit the rib/spar arrangement on swept wings to only two cases: (1) the ribs perpendicular to the spars or (2) the ribs parallel to the air flow. Both of those orientations are shown in Figure 1. Although both arrangements are mentioned in design textbooks the second arrangement is often disregarded because of weight concerns and no consideration is made for aeroleasticity. In research work the impact of the rib/spar arrangement was first explored by Harmin *et al*[16] who highlighted that rib/spar arrangement impacted the wing bend-twist coupling and hence its aeroelastic performance.

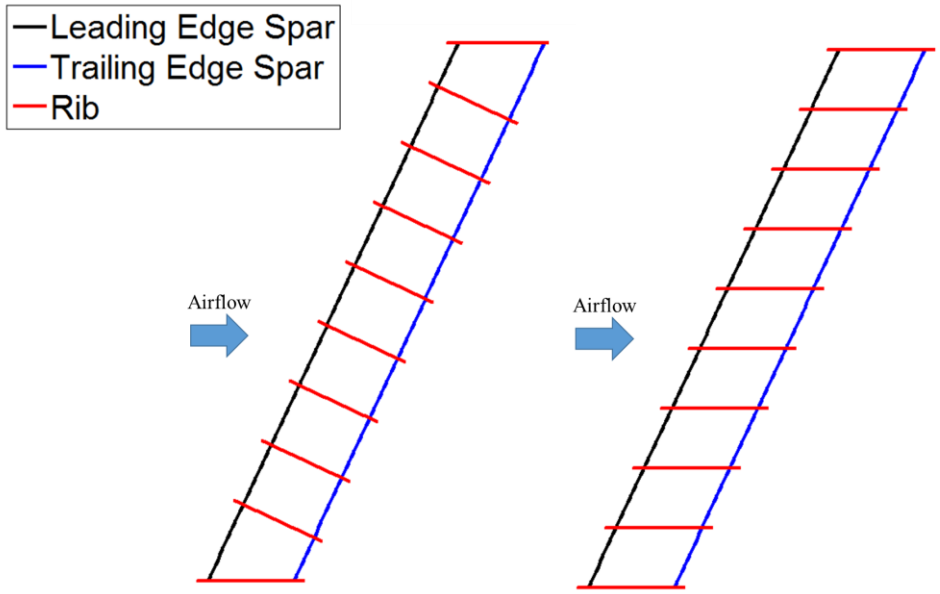

Figure 1. Design Textbook Rib Orientation for a Swept Back Wing.

B. Wing Model

All wings considered in this paper had a similar geometry. The wings were untapered and un-swept with a span of 500mm and a chord of 100mm. The aerofoil was a NACA 0012 profile. The wings internal structure were made of 8 ribs, 2 spars and a root and tip ribs closing the box. The leading and trailing edge spars were placed at 25% and 75% of the wing chord. The skin thickness was of 1mm and the rib and spar thickness changed with the orientation of the ribs to maintain a wing of constant mass. Additionally, to avoid the increase in skin panel size the change in rib orientation created a half rib at each end of the wing. The dimensions of the wings are shown in Figure 2 and the thicknesses summarised in Table 1. Since the wings were un-swept, the two classic rib/spar arrangements show in Figure 1 were similar: the ribs perpendicular to both spars and parallel to the airflow. In this paper this arrangement is referred to as the Base Case. The rib/spar arrangements explored in this paper are shown on Figure 3.

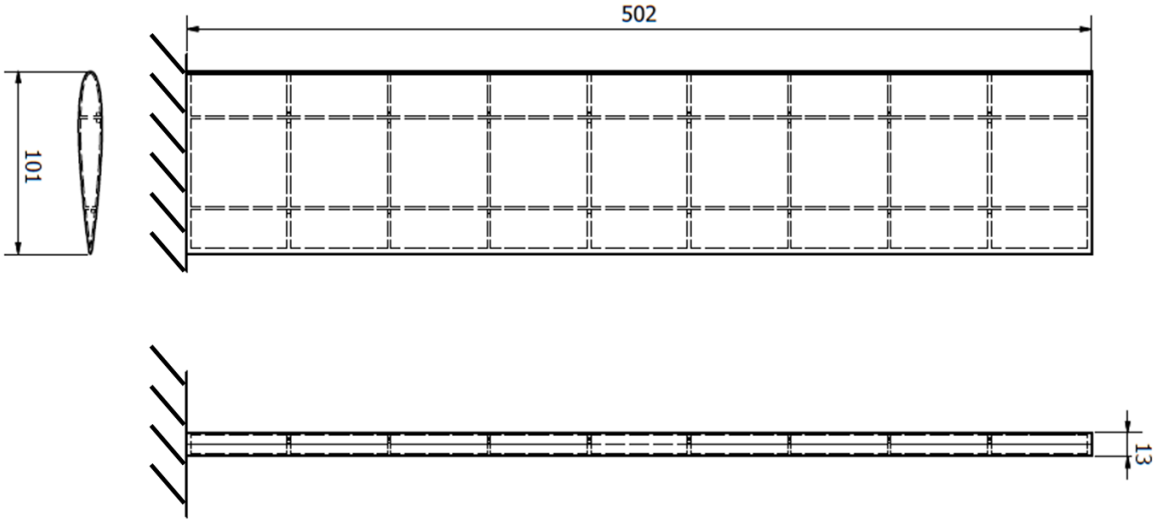

Figure 2. Wing Model External Dimensions in mm.

Table 1. Spar/Rib Arrangement and Corresponding Spar and Rib Thicknesses.

Rib Orientation (Degrees)	Spar Thickness (mm)	Rib Thickness (mm)
0 (Base Case)	2.00	2.00
15	1.88	1.88
-15	1.88	1.88
30	1.80	1.80
45	1.62	1.62

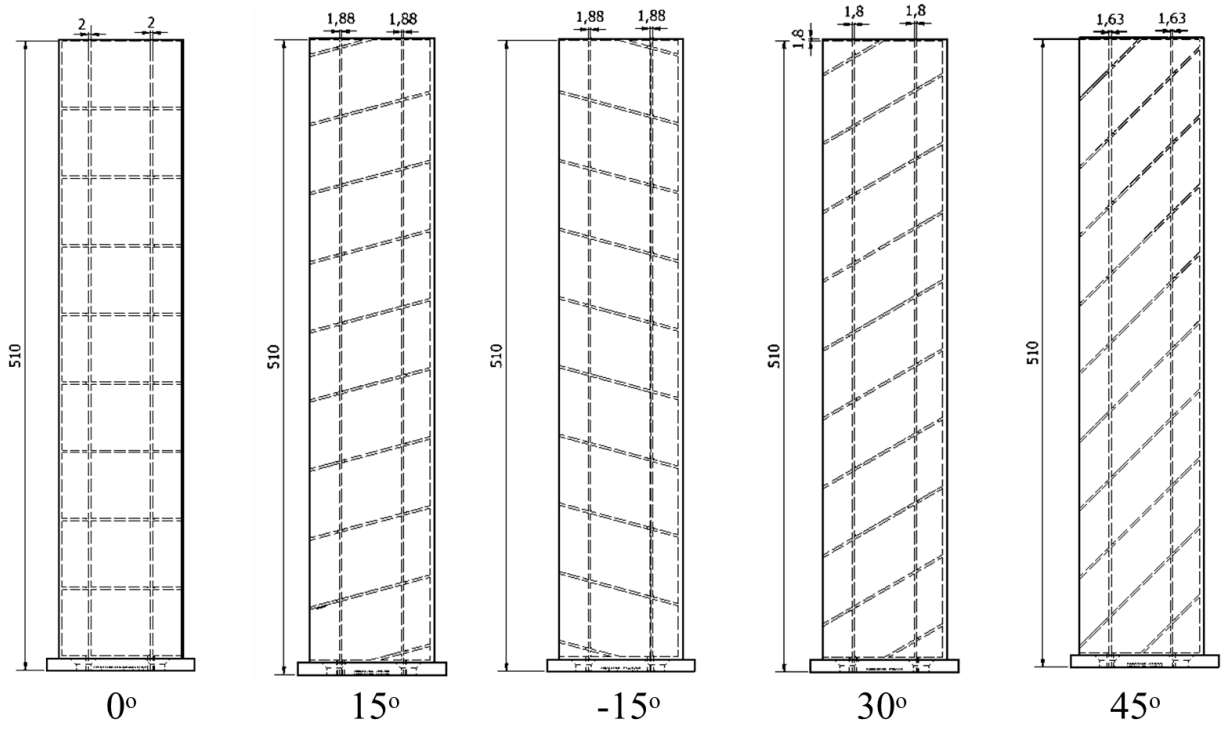

Figure 3. Rib/Spar Arrangement Explored in this Paper.

III. Structural Model

The impact of the rib/spar arrangement was first investigated using finite element (FE) modelling. The wing model shape and spar/rib arrangement was controlled in MATLAB and modelled in MSC.PATRAN. The material used was driven by the manufacturing of the wings and is specified in Section IV.

The geometry of the wing was specified in a MATLAB script that outputted a PATRAN session file to generate the FE model of the wing, which was then read by MSC.PATRAN. Actions include the creation of the surfaces, meshing of the surfaces, node equivalence and check of the element geometries as well as the creation of element properties and boundary conditions to be used in the different analyses. The geometry was meshed automatically in MSC.PATRAN using the IsoMesh meshing algorithm. The structure model was made using 2D shell elements. Initially, the wing model was built using quadrilateral shell elements (CQUAD4); however, these were replaced by triangular shell elements (CTRIA3) if their skew angle was less than 30°. It should be noted that the FE model made no simplification about the wing geometry, and so the curvature of the NACA aerofoil were fully considered and so required a high number of elements. The model mesh contained over 120,000 structural elements and 400 aerodynamic panels for the aeroelastic calculations.

The wings created underwent three different types of FE analysis: a static analysis, a modal analysis and an aeroelastic static analysis. The aim of these analysis was to model the behaviour of the wing in conditions similar to the experimental ones.

The static analysis (SOL 101) was performed to assess the deflection and twist of the different wings when subjected to static loading. Two different analysis were performed, and in both analysis the wing was assumed to be fully fixed at the root.

Initially, various loads were applied at the tip of the wing. These aimed at validating the FE model in a simple load case. The load was applied to the wing tip using a Multiple Point Constraint (MPC) slaving all the nodes on the tip aerofoil to a node placed at the mid chord and on a line between the trailing and leading edge. It should be noted that such load would generate a bending load and a torque as the shear centre of an aerofoil is around quarter chord.

Secondly, a static analysis was used to estimate the position of the Flexural Axis by applying a unit load at the leading and trailing edge at various sections along the wing. The flexural axis is the line connecting flexural centres which are a point on a wing section at which the application of a shear force creates no twist of that section with respect to the root[22,23].

The modal analysis (SOL 103) was used to estimate the natural frequencies of the different mode shape of the wings and so compare such results with the experimental ones. The wing was, once again, assumed to be fully fixed by the root.

The static aeroelasticity analysis (SOL 144) was performed at angles of attack ranging from 0 to 5° and at speed from 5m/s to 40m/s. This analysis assessed the deflection and twist of the wing under different aeroelastic loading. In this analysis the wing was assumed to be fully fixed at the root.

IV. Experimental Testing

A. Wing Manufacturing

Having designed a set of wings to be tested, the wings had to be manufactured quickly, efficiently and at a limited cost. Additionally, the manufacturing method had to provide sufficient freedom for the consideration of various structural configurations in this study and finally, the manufacturing route had to ensure that the wings were made in a material with enough structural stiffness for the different tests to be carried out. For these reasons it was decided that the wings would be laser sintered from polyamide powder. The harden polyamide powder was considered to have the material properties shown in Table 2 as specified by the manufacturer and was considered to be an isotropic material with a dimensional tolerance of 0.3mm.

Table 2. Cured Polyamide Material Properties as Specified by Manufacturer.

E (N/mm^2)	1,650.0
ν	0.4
ρ (kg/m^3)	1,150.0

Excess powder trapped in the rib bays was removed by the creation of three small holes at the connection of the spars and covers at the root. Since the wings were to be tested in a fully fixed root condition a rectangular root section was manufactured with every wings as shown by Figure 4. Finally, the wings were painted with white paint on both sides and black paint speckles were applied on one side of the wings as shown by Figure 5 to enable the use of Digital Image Correlation (DIC). Table 3 highlights the variation in weight among the different wings and with the application of the paint.

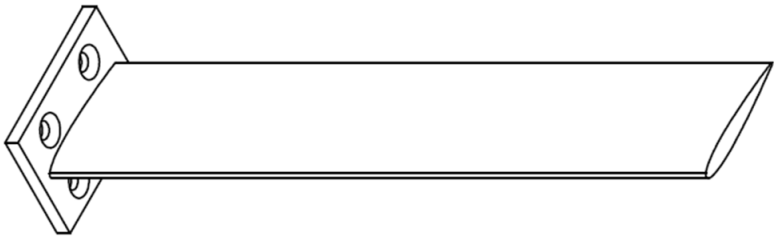

Figure 4. 3 View of the CAD File Sent to the Manufacturer with the Root Plate.

Figure 5. Illustration of the Black Speckle Pattern Applied on the Wings.

Table 3. Weight of the Wings without and With Paint.

Wing	Weight – No Paint (g)	Weight – With Paint (g)
Base Case	345	351
Rib @ 15°	324	332
Rib @ -15°	334	342
Rib @ 30°	327	336
Rib @ 45°	335	344

B. Static Testing

The static testing consisted of two different tests: (1) a static tip loading and (2) a static flexural axis loading. The loads were applied on the wing using the Load Application Device (LAD). The LAD consisted of a rectangular part with an opening of the shape of the wing aerofoil which is slightly larger than the wing aerofoil. This allowed the application of a load at various location along the span of the wing and yet provided a tight fit to prevent any motion of the LAD. The LAD is shown in Figure 6. In both tests, wing deflections were recorded using the 3D Digital Image Correlation (DIC) method –a contactless displacement measurement method. The DIC cameras were placed above the wings in order to measure the top side of the wings during these tests. The set up for the static testing is shown in Figure 7.

The first test (Static Experiment 1) examined the application of different tip loads and recorded whole wing deflection in all three axis. This test had for purpose to illustrate the behaviour of the different wings under static loading and also validate the FE model. The weight schedule is specified in Table 1. For every test point, three DIC images were captured.

The second test (Static Experiment 2) aimed to find the flexural axis by using the method described in Tathan[22] and Stodieck et al[23]. Loads were applied separately at the leading edge and then at the trailing edge of the wing. Two different weights (200 and 400g) were used for this test at the position specified in Table 4. The loads were always applied first at the trailing edge and then at the leading edge. The LAD was then moved to the new position and the procedure repeated. For every test point, three DIC images were taken.

Table 4. Mass Schedule for Static Experiment 1 and LAD Position from Root in Static Experiment 2.

Mass Applied (g) in Static Experiment 1											
0	105	245	350	451	554	654	758	858	963	1063	1167
LAD Position from Root (mm) in Static Experiment 2											
56		111		167		222		278	333	444	500

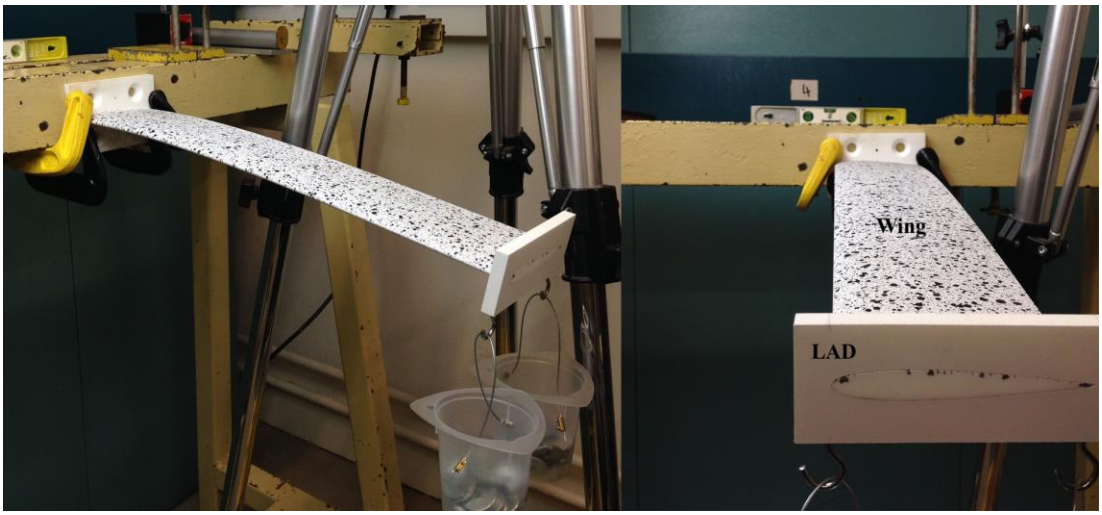

Figure 6. Load Application Device (LAD).

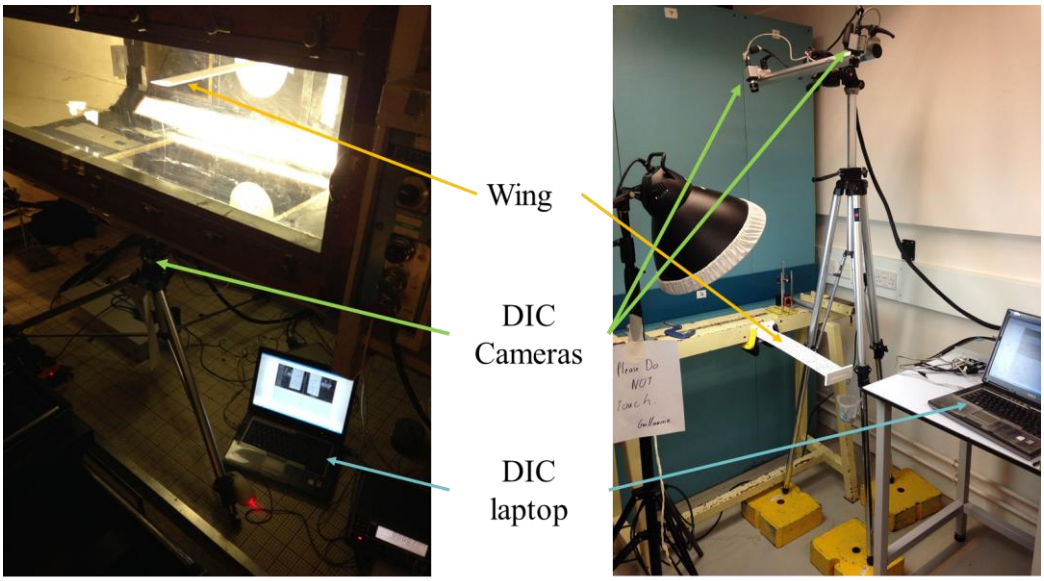

(a) Wind Tunnel Test (a) Static Test

Figure 7. Experimental Set-Up for the (a) Wind Tunnel Test and (b) the Static Test.

C. Wind Tunnel Testing

The wind tunnel test was used to measure the deflection of the wings under aerodynamic loading. The wings were placed horizontally in the wind tunnel and fixed to one wall. The DIC camera was placed outside the wind tunnel looking at the underside of the wings through a glass wall. The wind tunnel set up is shown in Figure 7.

The wings were fixed at a range of angle of attacks from 0^{o} to 5^{o} with 1^{o} increment and the wind tunnel speed was varied from 0m/s to 40m/s with 5m/s increment. At each test point three DIC images were captured.

D. Dynamic Testing

Dynamic testing was used to find the natural frequencies, damping ratios and the associated mode shapes. A "hammer" test was performed using a single accelerometer placed at the tip of the wing and impacting the structure at various impact points as shown by Figure 8 using five averages. The data measurement and analysis was performed using LMS International software.

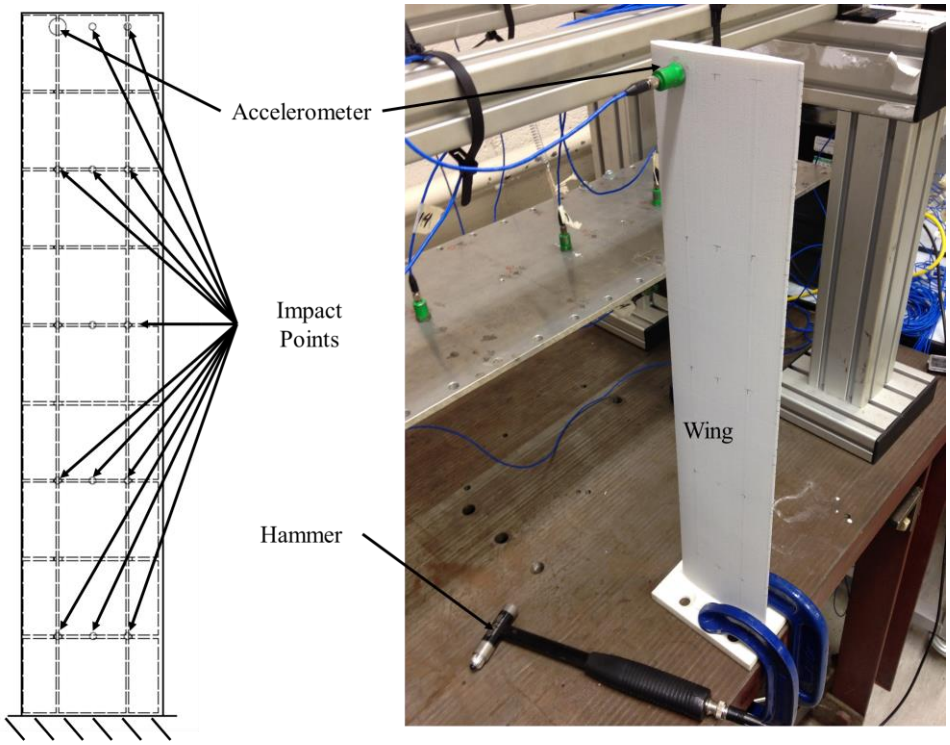

Figure 8. Accelerometer and Impact Locations and Dynamic Testing Set Up.

V. Results

The bending deflection for each test point was found by averaging the deflection found at the leading and trailing edge in both the FE modelling and by averaging the recorded points closest to the trailing and leading edge in the experiments. In the experiments, the displacement at particular points along the wings were found by surface fitting the point mesh data generated by the DIC system for every test points. This allowed the removal of any displacement inconsistency generated by the DIC system and also allowed computation of displacements at any point of interest on the wing.

The tip twist was found by measuring the difference in displacement on the trailing and leading edge in the FE modelling. In the experiments, the displacement at the leading and trailing edge was not available and thus the displacement at the points closest to the leading and the trailing edge were used to define the twist at a particular section and nose up twist is defined as positive.

The above calculations were performed for every DIC picture taken. A minimum of three pictures were taken for every test point. Hence in the following sections, the curve fitted line shown on plots results from a third order polynomial curve fit using every picture of every test points for a particular wing.

A. Static Loading – Tip Loading

In this section the experimental and modelling results for the different wings subjected to tip loads applied around the whole tip are presented. Figure 9 shows the increase in average tip deflection as the load is increased while Figure 10 details the variation in average tip deflection as the rib orientation is changed for the maximum load applied (1167g).

As shown by Figure 9 the different wings undergo different average tip deflection and a linear deflection as the load is increased as shown by the FE and test results. The FE modelling results display an increase in tip deflection for wings with a rib orientation different than zero. The Base Case wing has least deflection followed by the wing with ribs at successive angle of 15^{o}, 30^{o},-15^{o} and 45^{o} as shown in Figure 10. The experimental results also predict a change in tip deflection as the rib orientation is changed. Once again the Base Case wing sees the least tip deflection followed by the wing with ribs at successive angles of 15^{o}, 30^{o}, 45^{o} and -15^{o}.

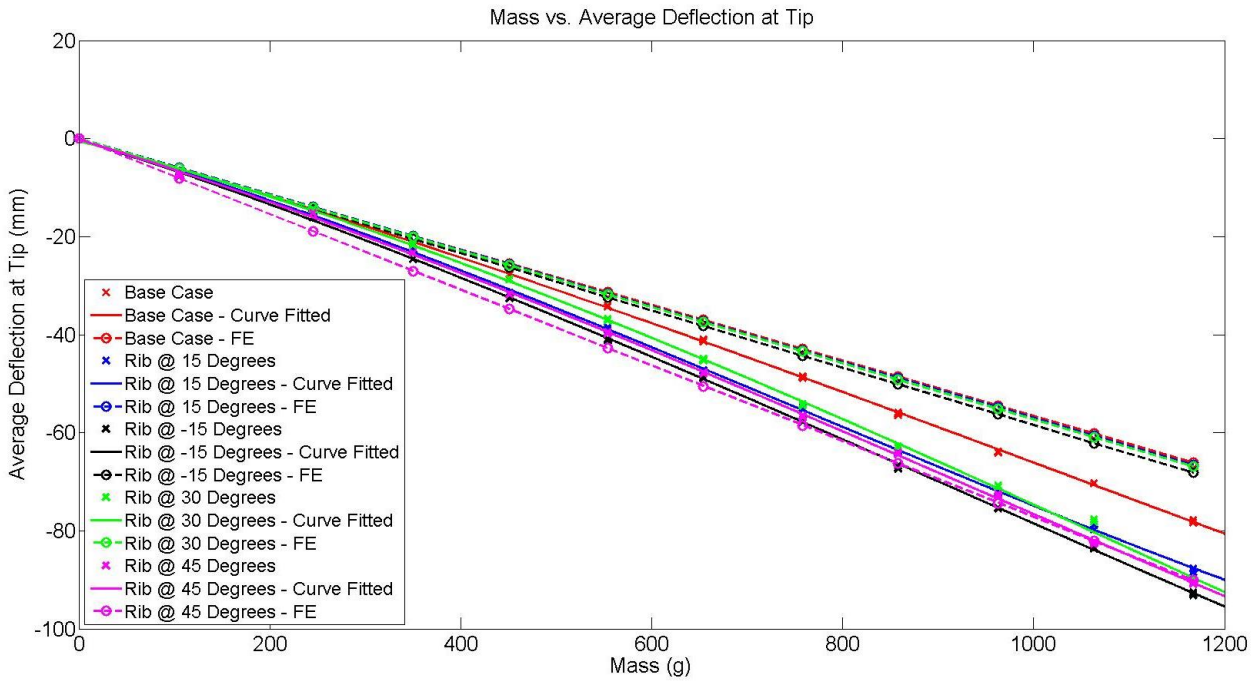

Figure 9. Average Tip Deflection due to Static Loads.

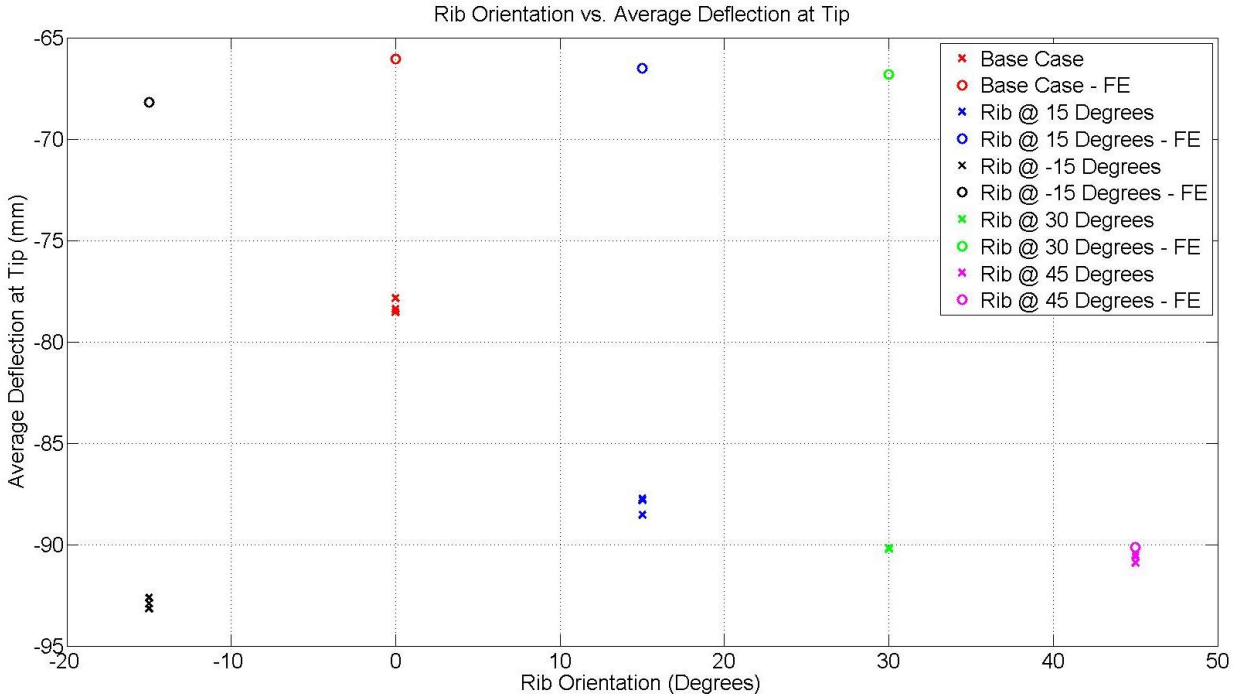

Figure 10. Average Deflection at Tip for Different Rib Orientation at a Load of 1167g.

Figure 11 shows the increase in tip twist as the load is increased while Figure 12 details the variation in tip deflection as the rib orientation is changed for the maximum load applied (1167g). The FE modelling results predict that the wing with ribs at -15°, 30°, 0° and finally ribs at 15° undergo an increase in nose down twist. Meanwhile the wing with ribs at 45° is predicted to undergo a nose up twist. Interestingly this variation in twist direction was not

found in the experimental results. In the experiment all the wings underwent a nose down twist. The twist was found to increase with the rib orientation as follows: ribs at 45°, 0°, -15°, 30° and finally 15°.

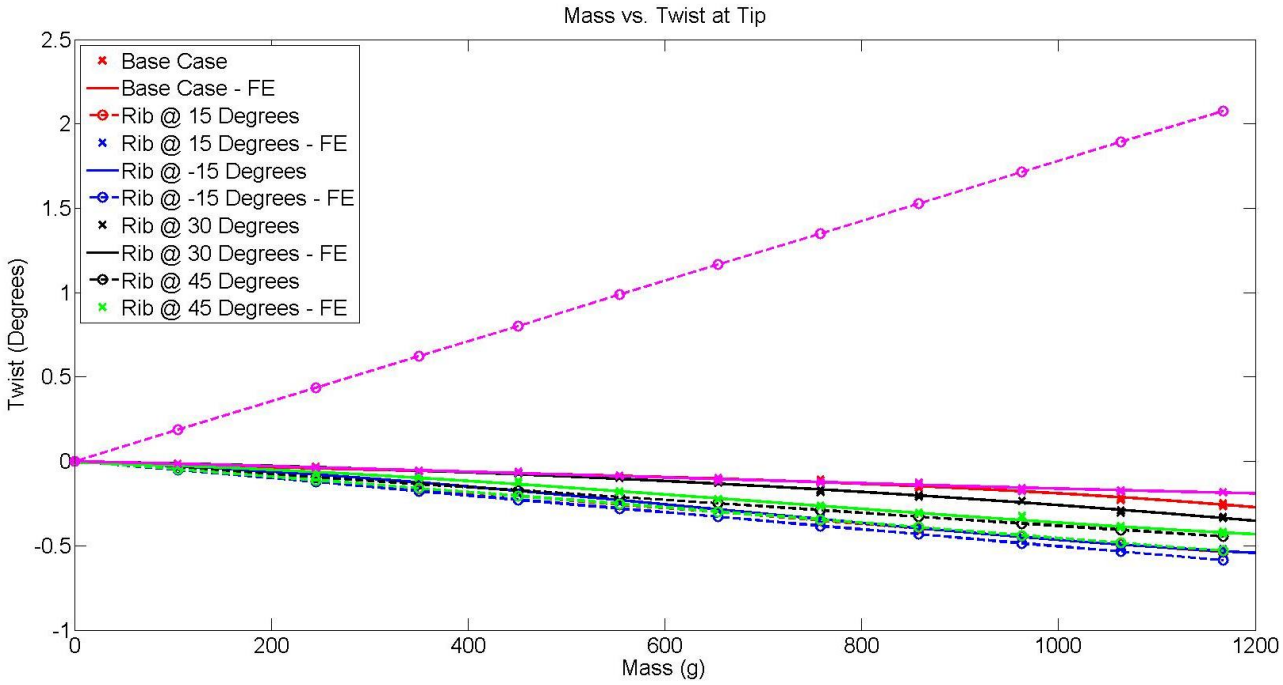

Figure 11. Tip Twist due to Static Loads. Nose up is Positive Twist.

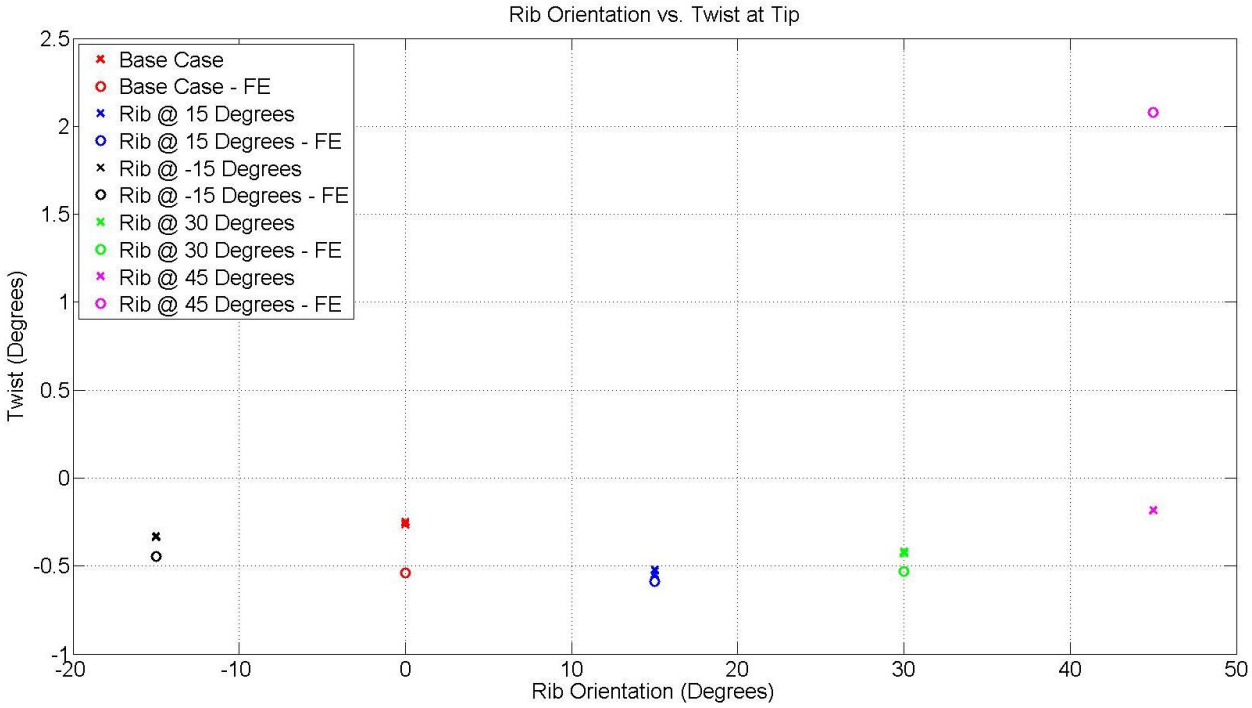

Figure 12. Twist at Tip for Different Rib Orientation at a Load of 1167g.

As shown by Figure 11 and Figure 12 some difference exists in tip displacement and twist between the FE and experiment results. A potential explanation for such differences is the material properties. Figure 13 shows the tip displacement and twist under maximum tip load for the Base Case wing with a 10% and 20% reduction in Young's

Modulus. Clearly, a reduction in material properties from the manufacturer values would explain part of the difference between the FE and experimental results. Additionally, manufacturing tolerances and experimental precision can explain some of the difference between the FE modelling and the experimental results.

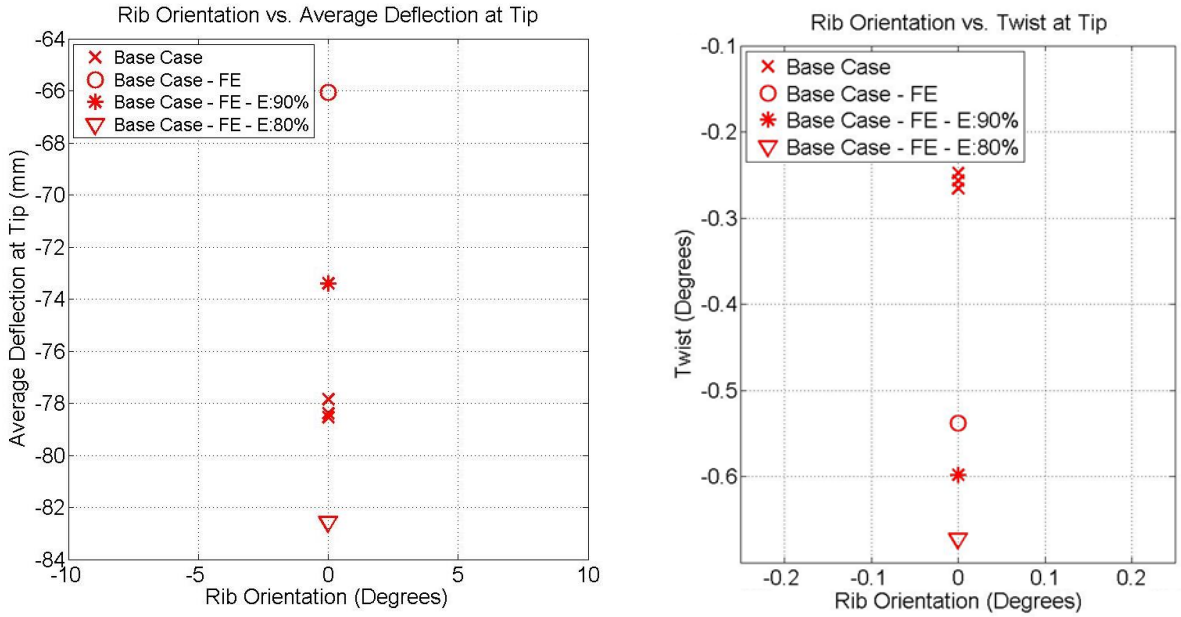

Figure 13. Tip Displacement and Twist for the Base Case Wing with Varying Young's Modulus.

B. Static Loading – Location of Flexural Axis

The aim of these tests was to evaluate the location of the flexural axis. In the modelling case, the vertical deflection of the nodes at a particular section was used to find out the twist of that section when subjected to a unit load at the trailing and leading edge. The location of flexural centre is then found by calculating the position on that section where a shear load results in no twist of the section. The FE modelling results of this analysis are presented in Figure 14.

In the experimental case, the vertical displacements ($\underline{r}$) of every sections along the wings for every load case ($\underline{R}$) considered were used to estimate the flexibility matrix (F) of the wing

$$\underline{r} = F\underline{R}$$

The flexibility matrix was then used to find the location of flexural centres. Those results are presented in Figure 15 and Figure 16.

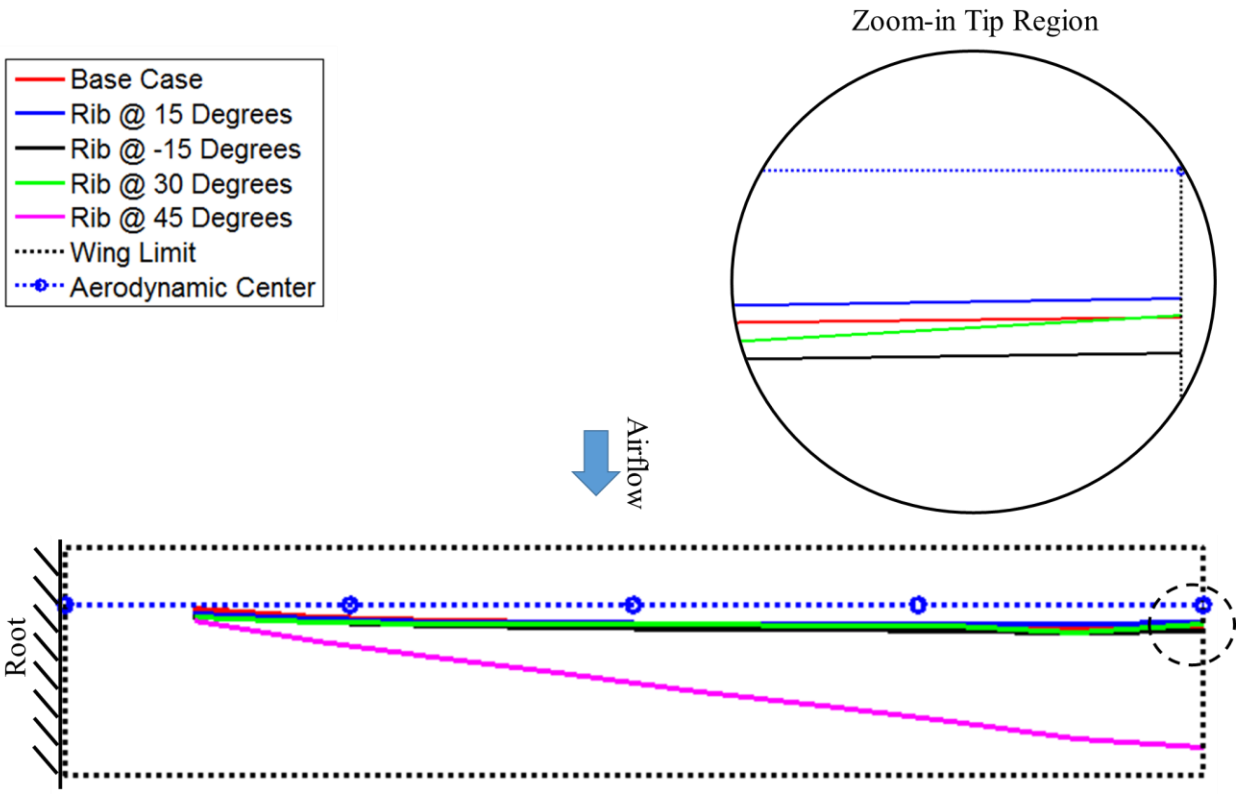

Figure 14. FE Modelling Flexural Axis Location for the Different Wings.

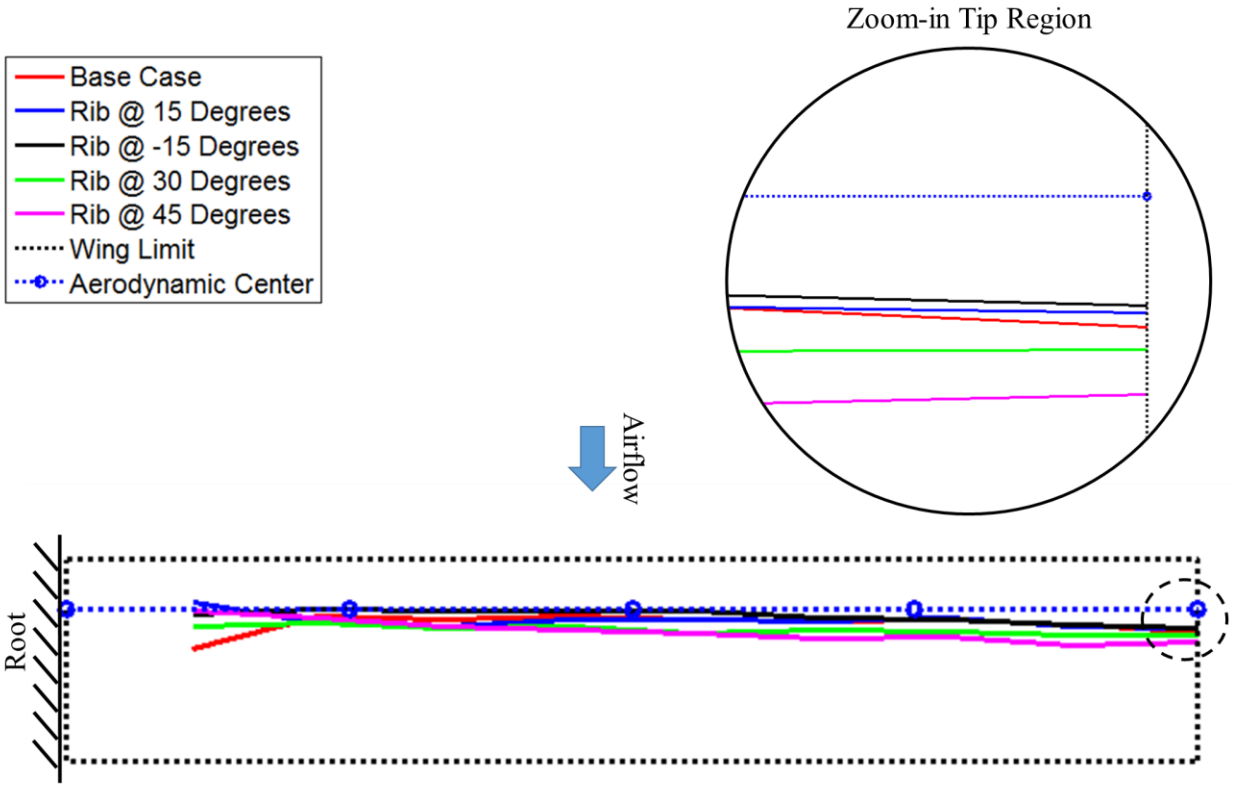

Figure 15. Experimental Flexural Axis Location for the Different Wings using a load of 200g.

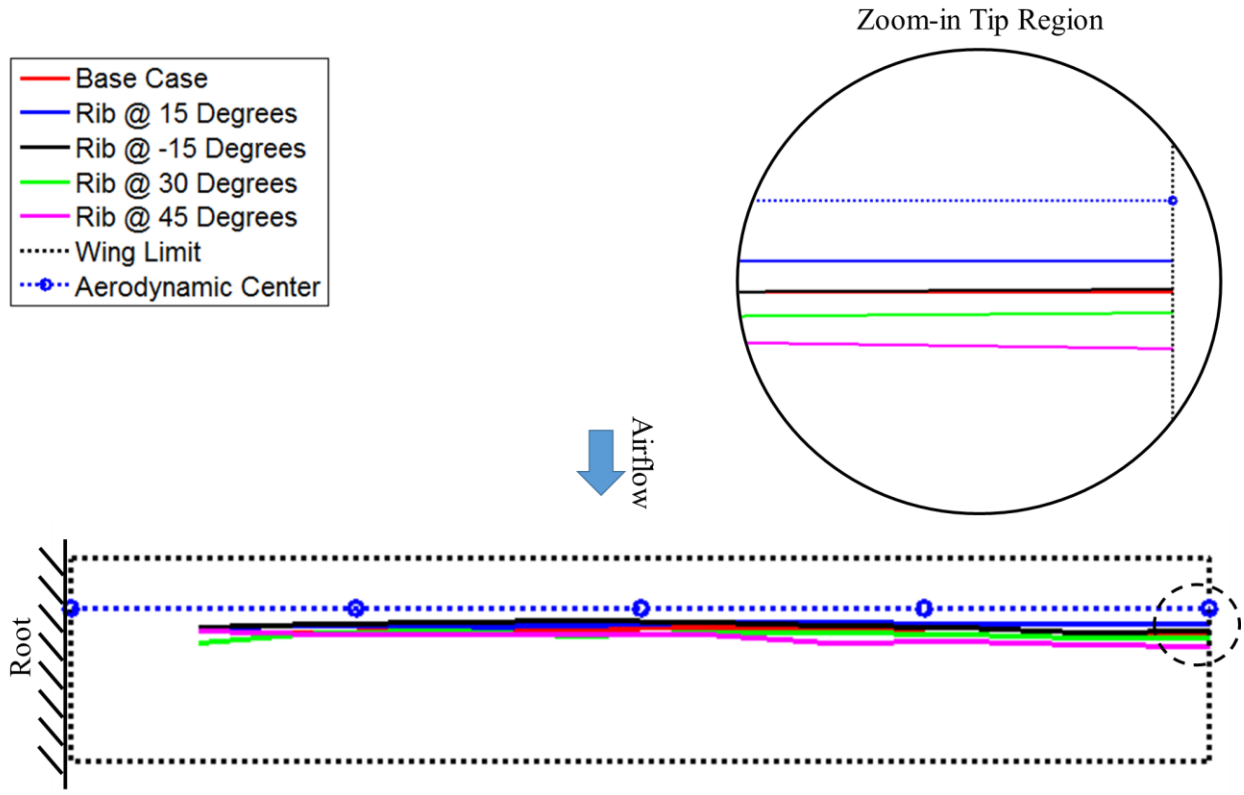

Figure 16. Experimental Flexural Axis Location for the Different Wings using a load of 400g.

The location of the flexural axis of the different wings, shown in Figure 14 for the FE modelling and Figure 15 and Figure 16 for the experiment, provides an explanation for the variation in bending and twist behaviour. For this discussion, the experimental results refer to Figure 16.

FE modelling predicted that the flexural axis at the tip of the wings is closer to the quarter chord when the ribs are placed at 15°, then 0°, then 30°, -15° and finally 45°. It should be noted that all the wings except the wing with ribs at 45° have a flexural axis in front of the mid chord. The application of a tip load at the mid chord creates a nose up moment resulting in a nose up twist for the wings with ribs at 0°,-15°, 15° and 30°. Similarly the application of a tip load at the mid chord for the wing with ribs at 45° translates in a bending force and a nose down moment.

The experimental results show that at the tip, the flexural axis is closer to the quarter chord point in the 15° wing, then -15°, 0°, 30° and finally 45° wing. Thus the flexural axis results for the wings that undergo highest and lowest twist correlate with the twist results found in the tip load experiment. It should be noted that none of the wings were found to have their flexural axis behind the mid chord point. Hence, for all wings the application of a load at the mid chord results in the generation of a bending force and nose down moment.

Although FE modelling and experimental results do not fully agree they both show that a change in rib orientation changes the location of the flexural axis which changes the structural bend-twist coupling of the wings suggesting that rib orientation can be used for aeroelastic tailoring purposes. However, it should be noted that the thickness of the spars and ribs were modified with the change in rib orientation so as to keep the wing mass constant. Thus to illustrate only the impact of the rib orientation on the coupling of the wing the flexural axis for the different wings was calculated by FE modelling on wings with ribs and spars of constant thickness of 2mm. The results of that analysis are shown in Figure 17 and show that small variation has a limited impact on the location of the flexural axis as compared to the impact provided by the change in rib orientation.

Manufacturing tolerances and experimental precision can explain some of the difference between the FE modelling and the experimental results.

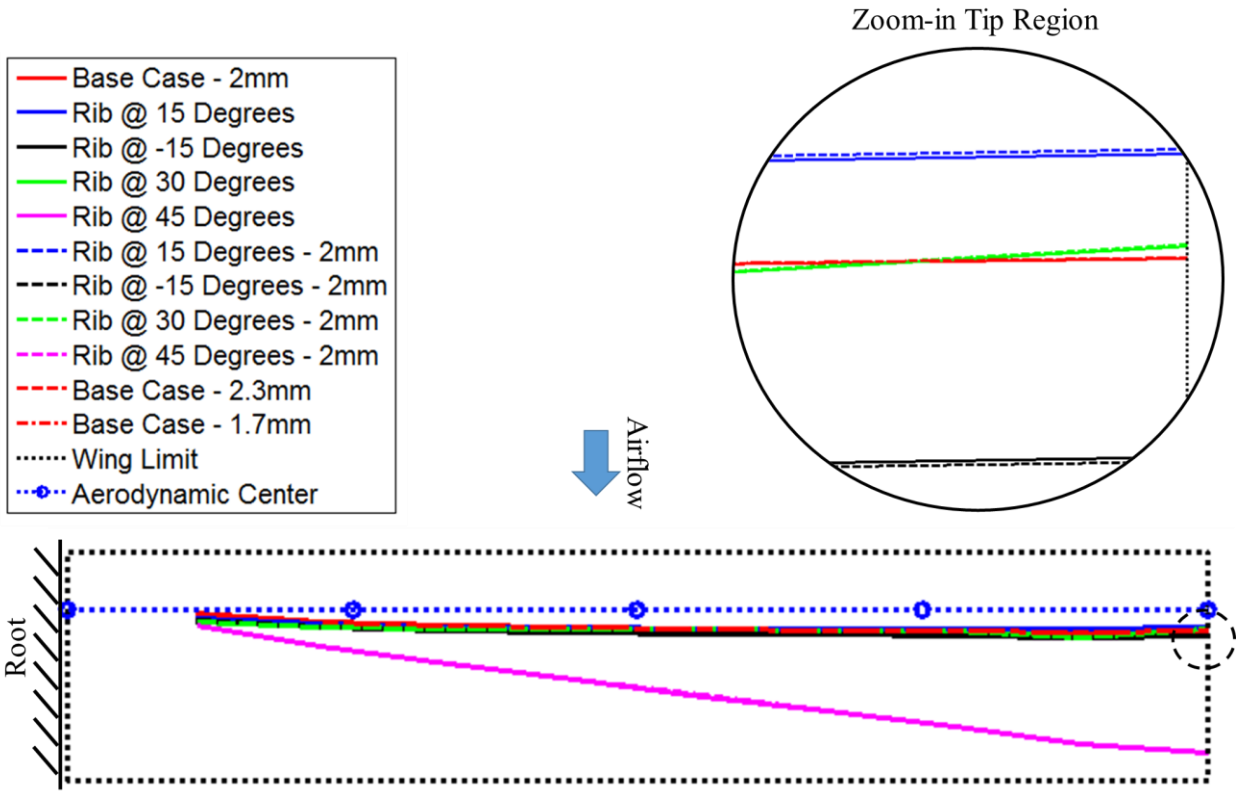

Figure 17. Flexural Axis Location of the Wings with Different Rib Orientation with Different Rib and Spar Thickness.

C. Aeroelastic Analysis

Figure 18 and Figure 19 show the modelling and experimental variation in average tip displacement and tip twist as the angle of attack is varied at an airspeed of 0m/s. The small variation in displacement recorded by the different DIC images at particular test points illustrates the impact of the vibration of the wind tunnel engine. Moreover, the fact that some of the data points are non-zero illustrates the precision of the DIC method and the data interpolation method applied on the DIC point mesh.

Figure 20 and Figure 21 show the modelling and experimental variation in average tip displacement and twist as the angle of attack is varied at an airspeed of 40m/s. Figure 20 and Figure 21 show that at an angle of attack of 0^{o} some tip deflection and twist were recorded. Since the wing has a symmetric aerofoil this should not occur. Thus this discrepancy in result is explained by the manufacturing tolerances and inaccuracy in the angle of attack setting.

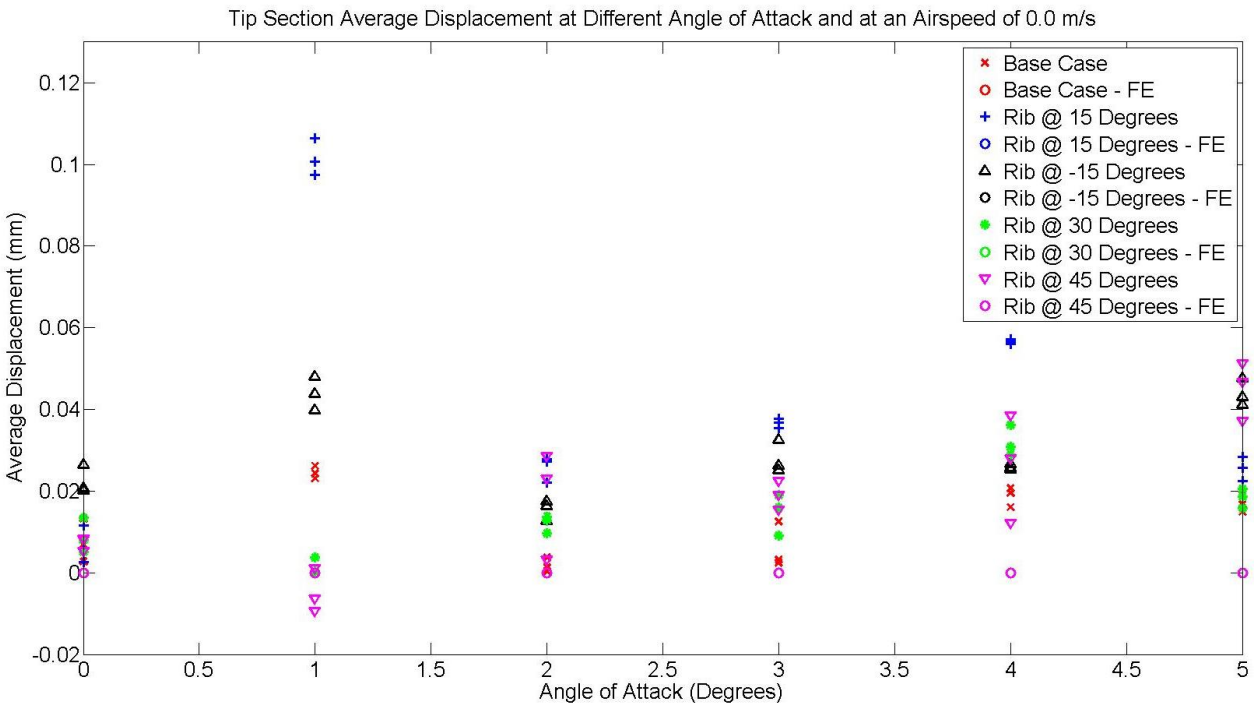

Figure 18. Average Displacement for Different Angle of Attack with an Airspeed of 0m/s.

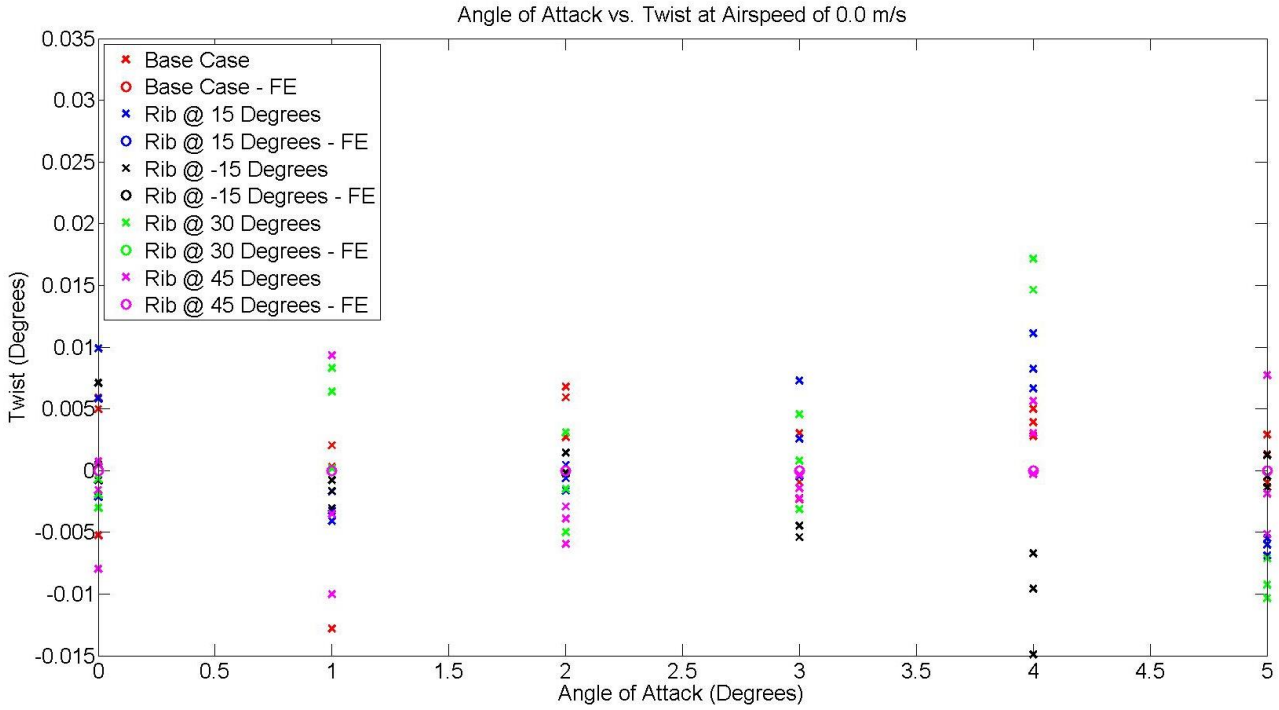

Figure 19. Tip Twist for Different Angle of Attack with an Airspeed of 0m/s.

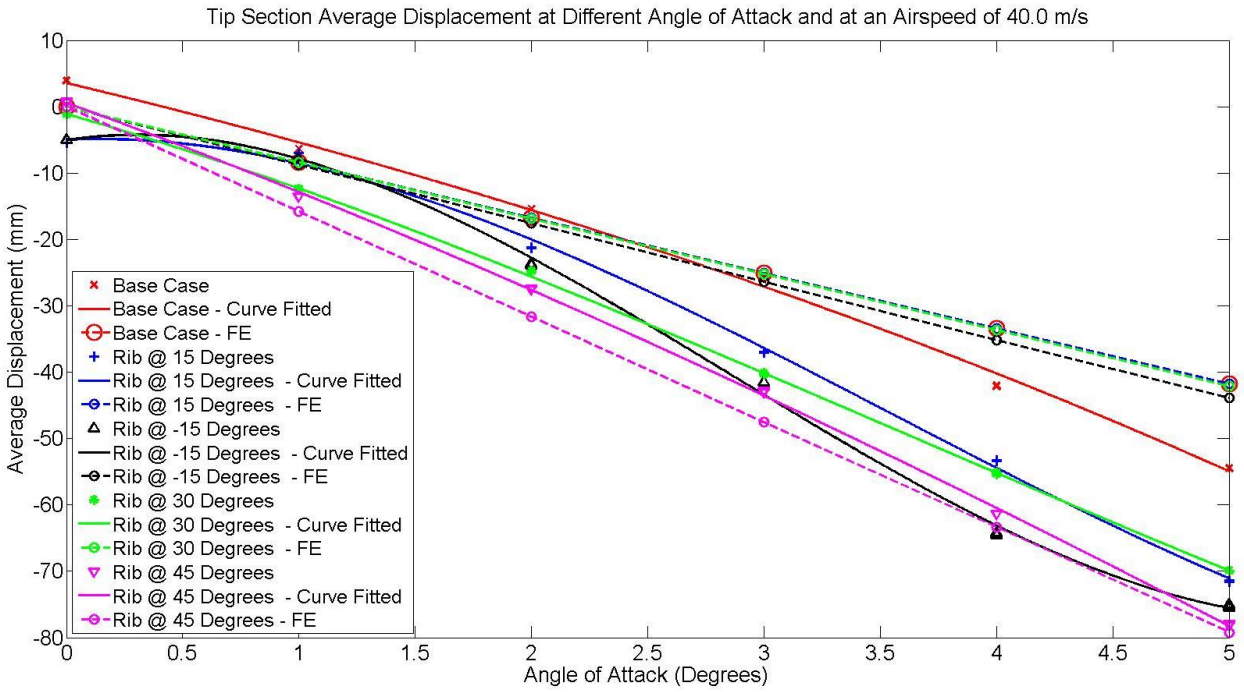

Figure 20. Average Displacement for Different Angle of Attack with an Airspeed of 40m/s.

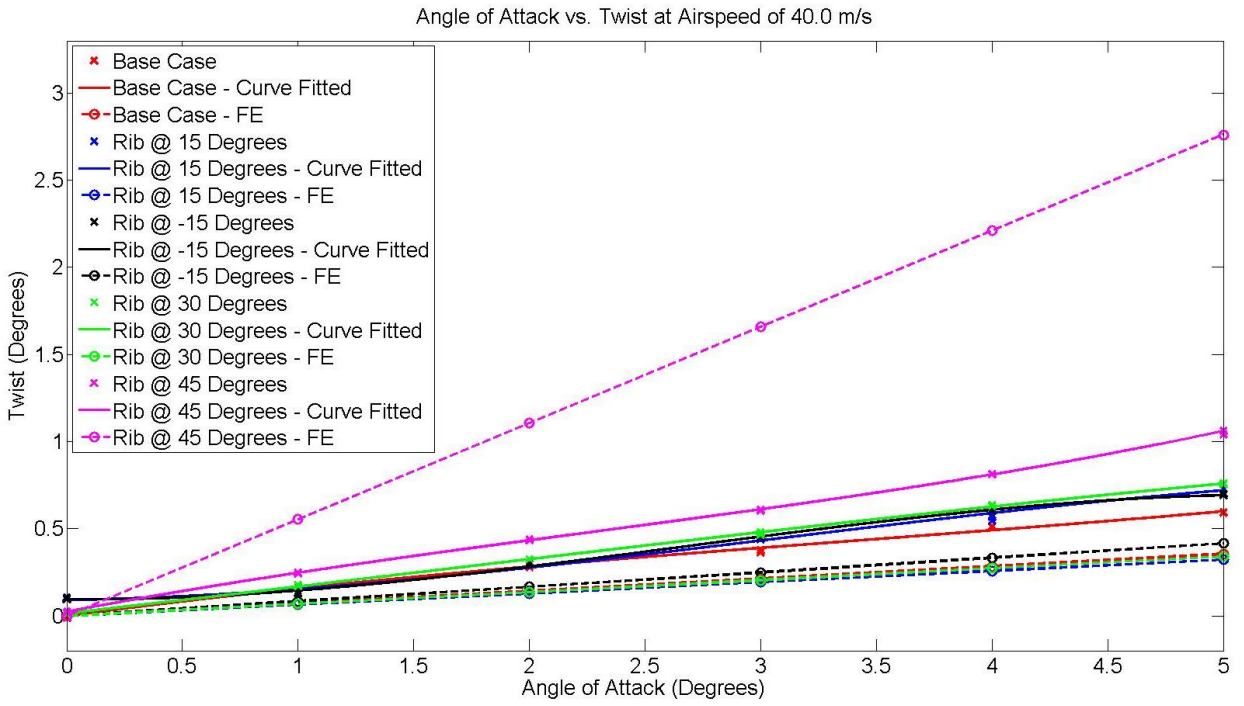

Figure 21. Tip Twist for Different Angle of Attack with an Airspeed of 40m/s.

Table 5, Table 6 and Table 7 present a ranking for the absolute tip displacement and the tip twist for every test point considered. In those tables, the maximum displacement/twist is noted by a 1 and the minimum displacement/twist is noted by a 5. Table 5 and Table 7 highlights the experimental deflection and twist behaviour of the different wings under aeroelastic loads. As the load increases, through higher airspeed and higher angle of

attack, it can be seen that a pattern appears: the wing with ribs at 45° experience the largest deflection and twist while the Base Case wing undergo the smallest deflection twist. Figure 21 shows that the wing with ribs at 45° undergoes larger twist while all the other wings are clustered around similar values. This behaviour is predicted by the FE models.

FE results shown in Figure 22, Figure 23 and in Table 6 show that the average tip deflection increases from the Base Case to the wing with rib at 15°, then 30° then -15° and finally rib at 45°. The tip twist is found to increase from the wing with rib at 15°, then 30°, then 0°, then -15° and finally 45°. It should be noted that the difference in average tip deflection and tip twist between the Base Case and the wings with ribs at 15°, -15° and 30° is at a maximum of –2.18mm and 0.16 degrees which are small when compared to the variation between the Base Case and the wing with rib at 45° (maximum of 37.47mm and 0.46 degrees). Such small variations are believed to be too small to be appropriately captured in the current experimental work. It should be noted that the FE results ranking does not vary with airspeed or a change in angle of attack.

The variation in average tip deflection and tip twist can once again be explained by looking at the flexural axis. The wing with ribs at 45° was found to have a flexural axis location the furthest aft implying maximum twist and deflection when a load is applied at the quarter chord.

Table 5. Ranking Matrix of the Average Tip Displacement Recorded During the Wind Tunnel Experiment. R0 is the Base Case.

	Airspeed (m/s)																				
	0					5					10					15					
Angle of Attack																					
0	1	3	5	2	4	1	4	2	3	5	2	4	5	1	3	2	3	1	4	5
1	2	3	1	5	4	1	2	3	4	5	4	3	5	2	1	5	4	3	2	1
2	3	5	1	4	2	1	3	2	4	5	4	5	3	2	1	3	5	4	2	1
3	2	5	1	4	3	3	5	4	2	1	4	5	3	2	1	1	5	4	3	2
4	4	5	1	2	3	1	4	5	3	2	1	5	3	4	2	1	5	3	4	2
5	2	5	3	4	1	1	4	5	2	3	1	5	3	4	2	1	5	3	4	2
Wings	R-15	R0	R15	R30	R45	R-15	R0	R15	R30	R45	R-15	R0	R15	R30	R45	R-15	R0	R15	R30	R45

	Airspeed (m/s)																				
	20					25					30					34					
Angle of Attack																					
0	3	2	1	5	4	3	2	1	5	4	3	2	1	5	4	2	3	1	4	5
1	5	4	3	2	1	5	4	3	2	1	5	4	3	2	1	5	4	3	2	1
2	4	5	3	2	1	3	5	4	2	1	3	5	4	2	1	3	5	4	2	1
3	3	5	4	2	1	3	5	4	2	1	2	5	4	3	1	2	5	4	3	1
4	1	5	3	4	2	1	5	4	3	2	1	5	4	3	2	1	5	4	3	2
5	1	5	3	4	2	1	5	3	4	2	2	5	3	4	1	2	5	3	4	1
Wings	R-15	R0	R15	R30	R45	R-15	R0	R15	R30	R45	R-15	R0	R15	R30	R45	R-15	R0	R15	R30	R45

Legend

Displacement	
Maximum	1
	2
	3
	4
Minimum	5

	Airspeed (m/s)										
	35					40					
Angle of Attack											
0	2	3	1	4	5	2	3	1	4	5	
1	3	5	4	2	1	3	5	4	2	1	
2	3	5	4	2	1	3	5	4	2	1	
3	2	5	4	3	1	2	5	4	3	1	
4	1	5	4	3	2	1	5	4	3	2	
5	2	5	3	4	1	2	5	3	4	1	
Wings	R-15	R0	R15	R30	R45	R-15	R0	R15	R30	R45	

Table 6. (a) Tip Displacement and (b) Twist Ranking Matrix for the FE Modelling Results during the Wing Tunnel Experiment. R0 is the Base Case.

	Airspeed (m/s)					Airspeed (m/s)				
	[5,10,15,20,25,30,34,35,40]					[5,10,15,20,25,30,34,35,40]				
Angle of Attack 0	5	5	5	5	5	5	5	5	5	5
Angle of Attack 1	2	5	4	3	1	2	3	5	4	1
Angle of Attack 2	2	5	4	3	1	2	3	5	4	1
Angle of Attack 3	2	5	4	3	1	2	3	5	4	1
Angle of Attack 4	2	5	4	3	1	2	3	5	4	1
Angle of Attack 5	2	5	4	3	1	2	3	5	4	1
Wings	R-15	R0	R15	R30	R45	R-15	R0	R15	R30	R45
	(a) Displacement					(b) Twist				

Table 7. Ranking Matrix of the Tip Twist Recorded during the Wing Tunnel Experiment. R0 is the Base Case.

	Airspeed (m/s)																			
	0					5					10					15				
Angle of Attack 0	2	5	1	4	3	3	2	1	4	5	2	3	1	4	5	2	4	1	5	3
Angle of Attack 1	4	2	3	1	5	3	5	4	1	2	2	5	4	1	3	4	3	5	2	1
Angle of Attack 2	5	1	4	3	2	1	2	3	5	4	4	3	2	5	1	5	3	2	4	1
Angle of Attack 3	1	5	2	4	3	5	3	4	2	1	5	3	4	2	1	4	5	3	2	1
Angle of Attack 4	2	4	3	1	5	3	5	4	1	2	5	3	4	2	1	5	4	3	2	1
Angle of Attack 5	5	3	2	1	4	5	2	3	4	1	2	4	5	3	1	4	5	3	2	1
Wings	R-15	R0	R15	R30	R45	R-15	R0	R15	R30	R45	R-15	R0	R15	R30	R45	R-15	R0	R15	R30	R45
	Airspeed (m/s)																			
	20					25					30					34				
Angle of Attack 0	2	3	1	5	4	1	5	2	3	4	2	4	1	5	3	2	5	1	3	4
Angle of Attack 1	4	3	5	2	1	4	3	5	2	1	4	3	5	2	1	4	3	5	2	1
Angle of Attack 2	2	4	5	3	1	3	5	4	2	1	3	5	4	2	1	4	5	3	2	1
Angle of Attack 3	3	5	4	2	1	3	5	4	2	1	3	5	4	2	1	3	5	4	2	1
Angle of Attack 4	3	4	5	2	1	3	5	4	2	1	3	5	4	2	1	3	5	4	2	1
Angle of Attack 5	4	5	3	2	1	4	5	3	2	1	4	5	3	2	1	4	5	3	2	1
Wings	R-15	R0	R15	R30	R45	R-15	R0	R15	R30	R45	R-15	R0	R15	R30	R45	R-15	R0	R15	R30	R45

Legend

Twist: Maximum 1; 2; 3; 4; Minimum 5

	Airspeed (m/s)									
	35					40				
Angle of Attack 0	2	5	1	3	4	1	5	2	3	4
Angle of Attack 1	4	3	5	2	1	4	3	5	2	1
Angle of Attack 2	3	5	4	2	1	3	5	4	2	1
Angle of Attack 3	3	5	4	2	1	3	5	4	2	1
Angle of Attack 4	3	5	4	2	1	3	5	4	2	1
Angle of Attack 5	4	5	3	2	1	4	5	3	2	1
Wings	R-15	R0	R15	R30	R45	R-15	R0	R15	R30	R45

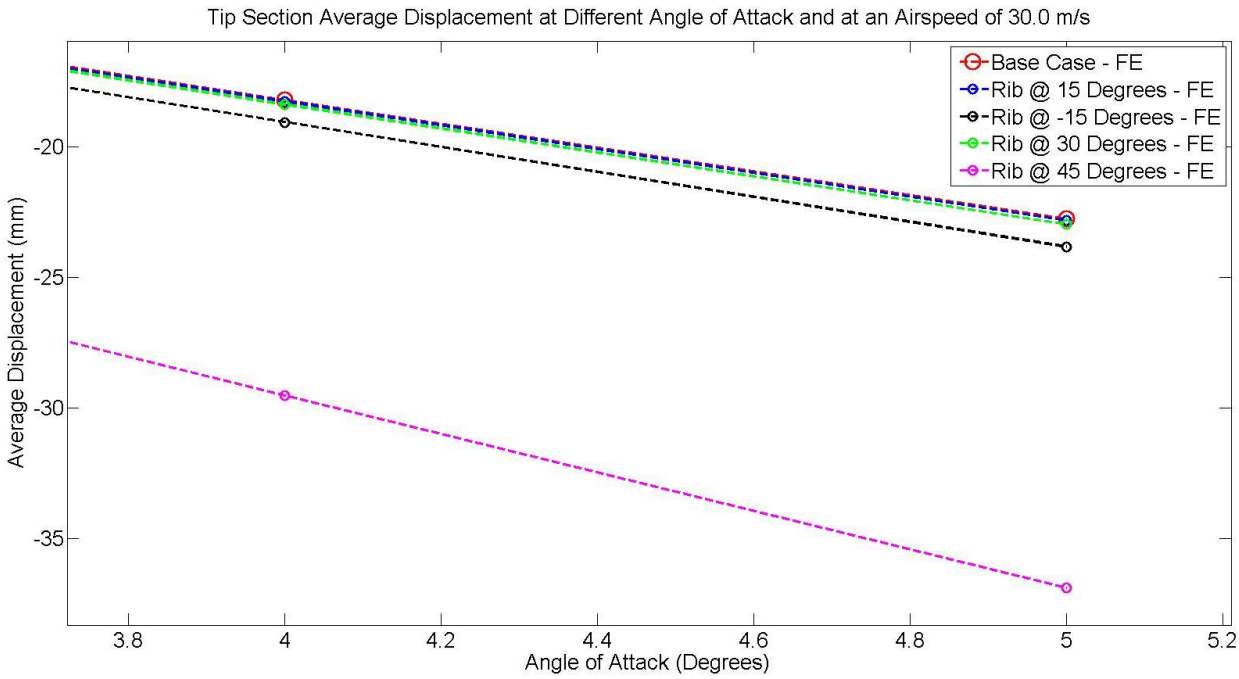

Figure 22. Zoom on the Tip Displacement for FE Results at an Airspeed of 30m/s.

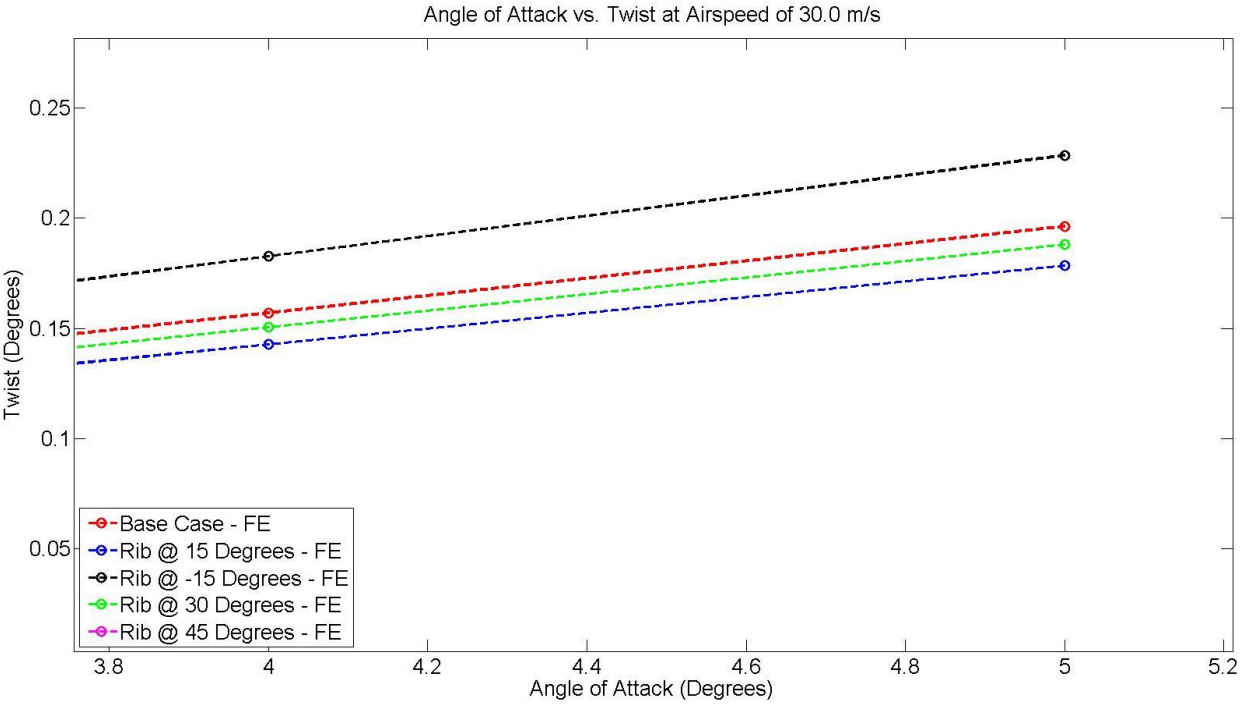

Figure 23. Zoom on the Tip Twist FE Results at an Airspeed of 30m/s.

D. Modal Analysis

Table 8 presents the natural frequencies, damping ratios and mode shape found through the experiment and an FE normal modes analysis. The difference in natural frequencies between the FE modelling and the experimental results are shown in Table 9, note that there is a significant difference between the two results in frequency but that the mode shapes are similar with the exception of a mixed mode that could not be detected by the experiment because of the positon of the accelerometer. Additionally, the consistency in difference in natural frequencies between in the FE and the experiment results suggests a good FE and experiment agreement. Once again the wing with the ribs at 45° has the smallest difference between the FE modelling and the experimental result as shown in Table 9.

Table 10 shows the variation in natural frequency for each mode with respect to the Base Case. It can be seen that natural frequencies change with the variation in rib orientation. FE modelling predicted that the largest change in natural frequencies occurs for a rib orientation of 45°, followed by rib at 30° and rib at -15° and finally rib at 15°. The experimental results suggest variation in natural frequencies is greater for rib -15°, 45°, 15° then ribs at 30°. The variation in weight for the different wings as shown in Table 3 could explain the lack of coherence in the experimental results. Nonetheless, it should be noted that the variation in natural frequencies by the change in rib orientation is found in both the experiment and the FE modelling suggesting that an increase in flutter speed through the control of the rib orientation is possible.

Table 8. Natural Frequencies, Damping and Mode Shape for the Different Wings Considered.

	R0 – Experiment			R0 – FE	
Mode	Freq (Hz)	Damping %	Shape	Freq (Hz)	Shape
1	7.64	4.81	Bending	10.66	Bending
2	47.51	1.2	Bending	64.00	Bending
				69.48	Mixed
3	80.58	2.53	Torsion	94.68	Torsion
4	128.92	2.02	Bending	169.12	Bending
5	233.39	3.12	Torsion	282.13	Torsion

	R15 – Experiment			R15 – FE		R-15 – Experiment			R-15 – FE	
Mode	Freq (Hz)	Damping %	Shape	Freq (Hz)	Shape	Freq (Hz)	Damping %	Shape	Freq (Hz)	Shape
1	7.22	3.74	Bending	10.55	Bending	7.12	2.17	Bending	10.43	Bending
2	46.03	1.48	Bending	63.44	Bending	45.62	2.06	Bending	62.97	Bending
				68.76	Mixed				67.49	Mixed
3	78.61	2.25	Torsion	95.16	Torsion	78.00	2.56	Torsion	94.52	Torsion
4	125.48	2.01	Bending	168.00	Bending	123.78	2.1	Bending	167.05	Bending
5	227.64	2.09	Torsion	283.16	Torsion	223.04	3.22	Torsion	281.73	Torsion

	R30 – Experiment			R30 – FE		R45 – Experiment			R45 – FE	
Mode	Freq (Hz)	Damping %	Shape	Freq (Hz)	Shape	Freq (Hz)	Damping %	Type	Freq (Hz)	Shape
1	7.36	3.2	Bending	10.54	Bending	7.25	3.1	Bending	9.15	Bending
2	46.41	1.41	Bending	63.47	Bending	45.58	1.32	Bending	54.58	Bending
				68.65	Mixed				67.55	Mixed
3	79.31	2.54	Torsion	96.07	Torsion	78.93	2.35	Torsion	84.81	Torsion
4	126.11	2.2	Bending	168.29	Bending	123.62	1.72	Bending	144.49	Bending
5	230.63	4.71	Torsion	285.69	Torsion	228.69	3.02	Torsion	253.77	Torsion

Table 9. Percentage Difference in Natural Frequencies between the Experimental and the FE Results.

	% Difference Between Experiment and FE				
Mode	R0	R15	R-15	R30	R45
1	-28.30	-31.60	-31.73	-30.18	-20.80
2	-25.77	-27.45	-27.55	-26.88	-16.50
	-100.00	-100.00	-100.00	-100.00	-100.00
3	-14.89	-17.39	-17.48	-17.45	-6.94
4	-23.77	-25.31	-25.90	-25.06	-14.45
5	-17.27	-19.61	-20.83	-19.27	-9.88

Table 10. Variation in Natural Frequencies between the Base Case (R0) and the Other Wings with the FE and the Experimental Results.

	% Difference with respect to R0 - FE				% Difference with respect to R0 - Experiment			
Mode	R15	R-15	R30	R45	R15	R-15	R30	R45
1	-0.99	-2.18	-1.09	-14.13	-5.55	-6.86	-3.68	-5.14
2	-0.87	-1.60	-0.83	-14.72	-3.12	-3.97	-2.31	-4.07
	-1.03	-2.86	-1.19	-2.78	0.00	0.00	0.00	0.00
3	0.51	-0.17	1.47	-10.42	-2.44	-3.20	-1.58	-2.05
4	-0.66	-1.22	-0.49	-14.57	-2.67	-3.99	-2.18	-4.12
5	0.37	-0.14	1.26	-10.05	-2.47	-4.44	-1.19	-2.02

VI. Conclusions

In this paper, the impact of rib orientation with respect to the spars was investigated through an experimental test programme in comparison with FE modelling. Wings with different rib orientation from -15° to 45° with 15° increment were considered with the wings manufactured using polyamide laser sintering. The wings were tested through: (1) static testing, (2) wind tunnel testing and (3) dynamic testing.

Although FE modelling and experimental work did not fully agree, both showed that the change in rib orientation modified the structural bend-twist coupling of the wings and so changed the wings' responses under static and aeroelastic loading. Those changes were related to a change in the flexural axis location. Additionally, both showed a change in the natural frequencies.

Future work will be dedicated to reducing the differences between the FE models and the experiments and to examine the effect of uncertainties in the manufacturing process. A better characterisation of the material properties, the physical wing weight distribution and shape will help in reducing this gap. To do so, the use of a four point bend test and methods such as X-ray and laser scanning of the wings to make a wing model will be considered.

Acknowledgments

The authors gratefully acknowledges the support of the EPRSC under its ACCIS Doctoral Training Centre grant, EP/G036772/1, the Royal Academy of Engineering and the EOARD. The authors would also like to thank Yusuf Mahadik and Eric Eckstein for their help to calibrate the DIC system, and Julian Londono for his help with the LMS International software.

References

1. Airbus. *Future Journeys 2013-2032*. (2013). at <http://www.airbus.com/company/market/forecast/?eID=dam_frontend_push&docID=33752>
2. Wright, J. R. & Cooper, J. E. *Introduction to Aircraft Aeroelasticity and Loads*. (Wiley, 2007).
3. Shirk, M. H., Hertz, T. J. & Weisshaar, T. A. Aeroelastic tailoring-theory, practice, and promise. *Journal of Aircraft* 23, 6–18 (1986).

4. Eastep, F. E., Tischler, V. A., Venkayya, V. B. & Khot, N. S. Aeroelastic tailoring of composite structures. *Journal of aircraft* 36, 1041–1047 (1999).
5. Kim, T. & Hwang, I. H. Optimal design of composite wing subjected to gust loads. *Computers & Structures* 83, 1546–1554 (2005).
6. Guo, S. Aeroelastic optimization of an aerobatic aircraft wing structure. *Aerospace Science and Technology* 11, 396–404 (2007).
7. Guo, S., Li, D. & Liu, Y. Multi-objective optimization of a composite wing subject to strength and aeroelastic constraints. *Proceedings of the Institution of Mechanical Engineers, Part G: Journal of Aerospace Engineering* 226, 1095–1106 (2011).
8. Manan, A., Vio, G. A., Harmin, M. Y. & Cooper, J. E. Optimization of aeroelastic composite structures using evolutionary algorithms. *Engineering Optimization* 42, 171–184 (2010).
9. Stodieck, O., Cooper, J. E. & Weaver, P. M. Optimisation of Tow - Steered Composite Wing Laminates for Aeroelastic Tailoring. in *53th AIAA/ASMe/ASCE/AHS/SC Structures, Structural Dynamics, and Material Conference, National Harbor, Maryland, USA* (2014).
10. Jutte, C. V, Stanford, B. K., Wieseman, C. D. & Moore, J. B. Aeroelastic Tailoring of the NASA Common Research Model via Novel Material and Structural Configurations. in *53th AIAA/ASMe/ASCE/AHS/SC Structures, Structural Dynamics, and Material Conference, National Harbor, Maryland, USA* 1–20 (2014).
11. Bendsøe, M. P. & Sigmund, O. *Topology Optimization Theory, Methods and Applications*. (Springer, 2003).
12. Maute, K. & Allen, M. Conceptual design of aeroelastic structures by topology optimization. *Structural and Multidisciplinary Optimization* 27, 27–42 (2004).
13. Brampton, C. J., Kim, H. A. & Cunningham, J. L. Level Set Topology Optimisation of Aircraft Wing Considering Aerostructural Interaction. in *12th AIAA Aviation Technology, Integration, and operations (ATIO) Conference and 14th AIAA/ISSM 17-19 September 2012, Indianapolis, Indiana, United States of America* 1–10 (2012).
14. Dunning, P. D., Stanford, B. K. & Kim, H. A. Aerostructural Level Set Topology Optimization for a Common Research Model Wing. in *10th AIAA Multidisciplinary Design Optimization Conference, 13-17 January 2014, National Harbor, Maryland, USA* 1–21 (2014).
15. Kolonay, R. M. & Kobayashi, M. H. Topology, Shape, and Sizing Optimization of Aircraft Lifting Surfaces Using a Cellular Division Method. in *13th AIAA/ISSMO Multidisciplinary Analysis Optimization Conference, Forth Worth, Texas, United States of America* (2010).
16. Harmin, M. Y., Ahmed, A. T. & Cooper, J. E. Aeroelastic Tailoring of Metallic Wing Structures. in *52nd AIAA/ASME/ASCE/AHS/ASC Structures, Structural Dynamics and Materials Conference, 4-7 April 2011, Denver, Colorado, United States Of America* 1–19 (2011).
17. Vio, G. A. & Fitzpatrick, I. R. Design of Composite Structures for Improved Aeroelastic Performance. *28th ICAS, 23-28 September 2012, Brisbane, Australia* 1–9 (2012).
18. Francois, G. & Cooper, J. E. Novel Structural Wing Designs for Forward Swept Wings. in *2014 Royal Aeronautical Society Biennial Applied Aerodynamics Research Conference, 22-24 July 2014, Bristol ,UK* 1–16 (2014).
19. Locatelli, D., Mulani, S. B. & Kapania, R. K. Wing-Box Weight Optimization Using Curvilinear Spars and Ribs (SpaRibs). *Journal of Aircraft* 48, 1671–1684 (2011).
20. Francois, G., Cooper, J. E. & Weaver, P. M. Aeroelastic Tailoring of Composite Wings using Internal Structural Members Shape and Stacking Sequence. in *Proceedings of the 4th Aircraft Structural Design Conference, 7-9 October 2014, Belfast, UK* (2014).
21. Niu, M. C. Y. *Airframe Structural Design*. (Hong Kong Conmilit Press Ltd, 1999).
22. Tatham, R. Shear Centre, Flexural Centre and Flexural Axis: An Attempt to Clear up Current Confusion and Provide Definitions Differentiating Between the Three Terms. *Aircraft Engineering and Aerospace Technology* 23, 209–210 (1951).
23. Stodieck, O., Cooper, J. E. & Weaver, P. M. On the Interpretation of Bending-Torsion Coupling for Swept, Non-Homogenous Wings. in *54th AIAA/ASMe/ASCE/AHS/SC Structures, Structural Dynamics, and Material Conference, Kissimmee, Florida, USA* 1–28 (2015).